1-1-2010

Measurement of the Interior Structure of Thin Polymer Films Using Grazing Incidence Diffuse X-Ray Scattering

Laurence Lurio

M.K. Mukhopadhyay

Zhang Jiang

X. Jiao

Michael Sprung

See next page for additional authors

Original Citation

M.K. Mukhopadhyay, L.B. Lurio, Z. Jiang, X. Jiao, M. Sprung, C DeCaro and S.K. Sinha, "Measurement of the interior structure of a thin polymer film using grazing incidence diffuse x-ray scattering" Phys. Rev. E 82, 011804 (2010)

Measurement of the interior structure of thin polymer films using grazing incidence diffuse x-ray scattering

M. K. Mukhopadhyay,[1] L. B. Lurio,[2] Z. Jiang,[1,3] X. Jiao,[3] Michael Sprung,[3] Curt DeCaro,[2] and S. K. Sinha[1]
[1]*Department of Physics, University of California–San Diego, La Jolla, California 92093, USA*
[2]*Department of Physics, Northern Illinois University, DeKalb, Illinois 60115, USA*
[3]*Advanced Photon Source, Argonne National Laboratory, Argonne, Illinois 60439, USA*
(Received 12 May 2010; published 30 July 2010)

A method is developed for calculating the small-angle x-ray scattering originating from within the interior of a thin film under grazing incidence illumination. This offers the possibility of using x-ray scattering to probe how the structure of polymers is modified by confinement. When the diffuse scattering from a thin film is measured over a range of incident angles, it is possible to separate the contributions to scattering from the interfaces and the contribution from the film interior. Using the distorted-wave Born approximation the structure factor, $S(q)$, of the film interior can then be obtained. We apply this method to analyze density fluctuations from within the interior of a silicon supported molten polystyrene (PS) film. Measurements were made as a function of film thickness ranging from one to ten times the polymer radius of gyration (R_g). The compressibility, calculated by extrapolating the measured $S(q)$ to $q=0$, agrees well with that of bulk PS for thick films, but thinner films exhibit a peak in $S(q)$ near $q=0$. This peak, which grows with decreasing thickness, is attributed to a decreased interpenetration of chains and a consequent enhanced compressibility.

DOI: 10.1103/PhysRevE.82.011804 PACS number(s): 82.35.Gh, 61.05.cm, 68.60.−p

I. INTRODUCTION

The effect of molecular scale confinement on the properties of a fluid is an issue of fundamental importance in condensed matter physics. This is of particular relevance in polymers since the molecular size, as characterized by the polymer radius of gyration, is several nanometers for high polymers. One of the most important tools used to study structural properties is small-angle x-ray scattering (SAXS) and this technique has found extensive use in studies of bulk fluids. SAXS measurements yield the structure factor, $S(q)$, which gives information on the density fluctuations and correlations. For thin films, experimental difficulties have made the use of SAXS measurements much less common. SAXS from within the interior of a thin film is weak and often overwhelmed by diffuse scattering from interfaces since the density contrast at an interface is generally much larger. This becomes a worsening problem as the film is made thinner since the intensity from bulk density fluctuations scales as the film thickness, whereas the surface scattering remains constant.

It was first suggested by Wang and Bedzyk [1] that x-ray standing waves set up within a surface film could be used to enable measurements of structure within the interior of the film. We have extended this method to enable the measurement SAXS from the interior of thin polymer films without interference from surface scattering. The system studied was a thin PS film on top of a Si substrate. The basis of the method relies on setting up a standing wave within the polymer film using grazing incidence x-rays. X-rays incident at angles below a materials critical angle α_c experience total external reflection. Since the critical angle for PS, $\alpha_{c,\mathrm{PS}}$, is less than that for Si, $\alpha_{c,\mathrm{Si}}$, there exists a range of incident angles where the x-rays penetrate the PS top layer and reflect from the Si. It is generally possible to find a condition where the standing wave has a node at the PS/vacuum interface and a maximum or several maxima within the interior of the film. Under these conditions scattering from the interior of the film will be preferentially excited. For very thin films, it is not possible to completely suppress the surface and interface scattering, but it is still possible to separate the contributions from the surface and interior via an analysis of the angular dependence of the scattering.

This paper is organized as follows: in Sec. II a theoretical formalism for calculating diffuse x-ray scattering under grazing incidence conditions is discussed. Here, the standard formalism which has generally been applied to the case of surface scattering is extended to describe scattering from the interior of a film. In Sec. III the results of SAXS from thin polystyrene films are presented. These results are analyzed in the context of the formalism developed in Sec. II. In Sec. IV wide-angle scattering (WAXS) results are presented. Finally in Sec. V the information obtained from SAXS and WAXS are compared and the implications for the structure of thin polymer films are discussed. In addition, the benefits and limitations of the technique of grazing incidence interior diffuse scattering are reviewed.

II. THEORETICAL FORMALISM

A formalism for calculating diffuse surface scattering in reflection geometry using the distorted-wave Born approximation (DWBA) was first worked out by Sinha *et al.* [2]. The DWBA was extended to the case of interior density fluctuations below a single interface by Rauscher *et al.* [3] and to the case of surface scattering from multiple interfaces by Holy *et al.* [4]. A good summary of the formalism is provided in the book by Tolan [5]. In the present work we extend the method of the DWBA to interior scattering from thin films. A schematic of the diffuse scattering experimental setup from thin films is shown in Fig. 1. In the thin film geometry there are two significant differences from the case

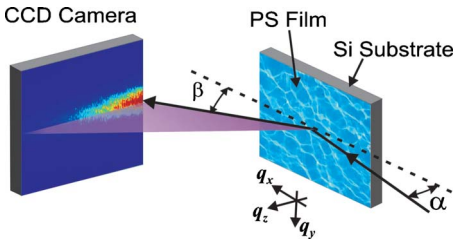

FIG. 1. (Color online) Schematic of the diffuse scattering setup.

examined by Rauscher *et al.* First, due to the interference set up by the standing wave within the film, for certain incident angles the surface scattering can be almost completely suppressed. Second, there is a spatially varying electric field in the surface normal direction due to the standing wave. This spatially varying field will produce scattered radiation in a method analogous to the scattering produced by a spatially varying electron density.

We begin by outlining the DWBA along the lines given by Rauscher *et al.* Since the scattering angles involved are all small, we can simplify the calculations by assuming a scalar electric field. The amplitude of the electric field satisfies the wave equation;

$$[\nabla^2 + k^2 - V_1(\vec{r}) - V_2(\vec{r})]\psi(\vec{r}) = 0. \tag{1}$$

Here $k=2\pi/\lambda$ is the x-ray wave vector, with λ as the wavelength. The function $V_1(\vec{r})$ represents the scattering potential of the idealized surface. This is given by $V_1(z)=k_c^2(z)$ with k_c as the critical wave vector within the material at height z as indicated in Fig. 2. This can be related to the electron density via $k_c^2=k^2(1-n^2)\approx 4\pi r_0\rho(z)$. Here $\rho(z)$ is the electron density of the material. The term $V_2(\vec{r})$ represents the perturbation from the idealized electron density due to surface/interface roughness and interior density fluctuations.

The method of the DWBA relies on the existence of a known solution to Eq. (1) for the case of $V_2(\vec{r})=0$. This is given by (see, e.g., Tolan [5])

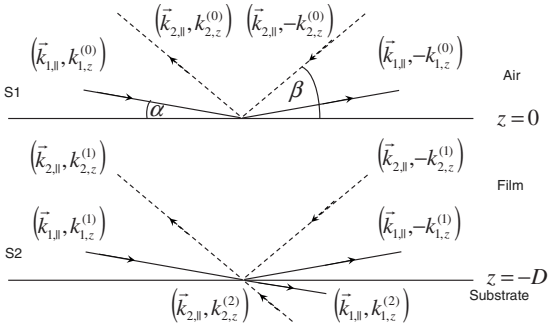

FIG. 2. Schematic of a air-film-substrate system. α is the incidence angle of the x-ray beam, β is the detector angle, and D is the film thickness.

$$\psi_1 = \begin{cases} e^{i\vec{k}_1^{(0)}\cdot\vec{r}} + R(\alpha)e^{i\vec{k'}_1^{(0)}\cdot\vec{r}} & \text{I} \\ A_1(\alpha)e^{i\vec{k}_1^{(1)}\cdot\vec{r}} + A_2(\alpha)e^{i\vec{k'}_1^{(1)}\cdot\vec{r}} & \text{II} \\ T(\alpha)e^{i\vec{k}_1^{(2)}\cdot\vec{r}} & \text{III} \end{cases}. \tag{2}$$

Here region I corresponds to the vacuum ($z>0$), region II corresponds to the film ($-D<z<0$), and region III corresponds to the substrate ($z<-D$). The incident wave vector in vacuum is $\vec{k}_1^{(0)}$ and the primed value is the specularly reflected wave vector defined by $\vec{k}_{1,\parallel}^{(0)}=\vec{k}'^{(0)}_{1,\parallel}=\vec{k}_{1,\parallel}$ and $\vec{k}_{1,z}^{(0)}=-\vec{k}'^{(0)}_{1,z}$. Here the subscript $\parallel$ refers to the component of the vector in the x-y plane. The corresponding values for the scattered wave are $\vec{k}_2^{(0)}$, $\vec{k}_2^{(1)}$, and $\vec{k}_2^{(2)}$.

The functions $R(\alpha)$ and $T(\alpha)$ are the Fresnel reflection and transmission coefficients, respectively, for the incidence angle α. $A_1(\alpha)$ and $A_2(\alpha)$ are the amplitudes of the electric field within the film. The superscripts (1) and (2) refer to the wave vectors in the film and substrate, respectively, with the primed and unprimed wave vectors bearing the same relation to each other as they do in the vacuum.

Following the dynamical theory of x-ray reflection [5–7], for a uniform layer of film on substrate, these coefficients are given as

$$R = \frac{r_{0,1} + r_{1,2}\exp(2il_1^{(0)}D)}{1 + r_{0,1}r_{1,2}\exp(2il_1^{(0)}D)},$$

$$T = \frac{(1+r_{0,1})(1-R)}{(1-r_{0,1})(1-r_{1,2})}\exp[-i(l_1^{(1)} - l_1^{(0)})],$$

$$A_1 = \frac{1 - Rr_{0,1}}{1 - r_{0,1}},$$

$$A_2 = \frac{R - r_{0,1}}{1 - r_{0,1}}, \tag{3}$$

where

$$r_{0,1} = \frac{l_1^{(0)} - l_1^{(1)}}{l_1^{(0)} + l_1^{(1)}},$$

$$r_{1,2} = \frac{l_1^{(1)} - l_1^{(2)}}{l_1^{(1)} + l_1^{(2)}}. \tag{4}$$

Here $l_1^{(0)} \equiv k_{1,z}^{(0)}$, and within the film we have $l_1^{(1)} = \sqrt{(l_1^{(0)})^2 - k_{c,f}^2}$. Here $k_{c,f}$ is the critical wave vector corresponding to the average electron density of the film ρ_f. The quantities $l_2^{(0)}$ and $l_2^{(1)}$ are the corresponding quantities for the scattered wave vector.

In the absence of a perturbation, an incident plane wave of the form $\phi=e^{i\vec{k}_i^{(0)}\cdot\vec{r}}$ will scatter into the state ψ_1. Note that this is an eigenstate of Eq. (1) for $V_2=0$ which satisfies $(\nabla^2+k^2)\psi_1 = V_1\psi_1$.

In the presence of the perturbing potential V_2 the incident wave ϕ may also scatter into other eigenstates. In particular, we are interested in the scattering cross section for x-rays to go into an outgoing wave along some direction k_2. In order to calculate this cross section we need to find the amplitude for

scattering into an eigenstate of the unperturbed equation which has this outgoing wave as its far-field limit. Since a time-reversed solution of the form of Eq. (2) is also an eigenstate of Eq. (1) and since this eigenstate has the required far-field form, we look at scattering into an eigenstate given by:

$$\tilde{\psi}_2 = \begin{Bmatrix} e^{ik_2^{(0)}\cdot\vec{r}} + R^*(\beta)e^{i\vec{k}_2'^{(0)}\cdot\vec{r}} & \text{I} \\ A_1^*(\beta)e^{i\vec{k}_2^{(1)}\cdot\vec{r}} + A_2^*(\beta)e^{i\vec{k}_2'^{(1)}\cdot\vec{r}} & \text{II} \\ T^*(\beta)e^{i(\vec{k}_2^{(2)})\cdot\vec{r}} & \text{III} \end{Bmatrix}. \quad (5)$$

If $k_2 \neq k_1$, corresponding to diffuse scattering, then the scattering cross section into the direction defined by k_2 is given by

$$\frac{d\sigma}{d\Omega} = \frac{1}{16\pi^2}\langle|\langle\tilde{\psi}_2|V_2|\psi_1\rangle|^2\rangle. \quad (6)$$

Here the outer brackets indicate a statistical averaging over the sample configurations. This forms the basic result of the DWBA.

The perturbing potential V_2 can be considered to be made up of three distinct parts: roughness at the film/vacuum interface, roughness at the film substrate interface, and diffuse scattering from the interior of the film. We can thus write

$$V_2 = V_{\text{surf}} + V_{\text{int}} + V_{\text{subs}}.$$

Using the shorthand to represent the matrix elements

$$\langle\psi_2|V_{\text{int}}|\psi_1\rangle = V_{\text{int},12},$$

etc. We can rewrite the term in Eq. (6) as

$$\langle|V_{\text{surf},12} + V_{\text{int},12} + V_{\text{subs},12}|^2\rangle = \langle|V_{\text{surf},12}|^2\rangle + \langle|V_{\text{int},12}|^2\rangle + \langle|V_{\text{subs},12}|^2\rangle + \langle\text{crossterms}\rangle. \quad (7)$$

Here, again, the brackets represent averaging over sample configurations.

In order to make the analysis tractable, we will assume that these three forms of roughness are uncorrelated and thus the cross terms average to zero. Then we can write for the scattering cross section:

$$\left.\frac{d\sigma}{d\Omega}\right|_{\text{diffuse}} = \left.\frac{d\sigma}{d\Omega}\right|_{\text{surf}} + \left.\frac{d\sigma}{d\Omega}\right|_{\text{subs}} + \left.\frac{d\sigma}{d\Omega}\right|_{\text{interior}}. \quad (8)$$

The term due to the surface fluctuations at the air-film interface has already been calculated elsewhere [2,4] and the differential scattering cross section can be written as

$$\left.\frac{d\sigma}{d\Omega}\right|_{\text{surf}} = r_o^2\rho_f^2 A_{xy}|E_{\text{in}}(0)|^2|E_{\text{out}}(0)|^2 S_c(\vec{q}). \quad (9)$$

Here A_{xy} is the illuminated area of the sample and $E_{in}(0)$ and $E_{out}(0)$ are the electric fields (normalized with respect to the incident beam) at the vacuum-polymer film interface (i.e., at $z=0$ in Fig. 2) that would be created if the beam were incident at either the angle of incidence or detection, respectively, as calculated using the dynamical matrix formalism of Parratt [7]. $S_c(\vec{q})$ is the structure factor corresponding to the surface height-height correlations which can be well approximated by the capillary-wave fluctuations at the surface of the polymer films [8,9]. Similar to the surface term, the contribution due to the substrate roughness at the film substrate interface can be written as

$$\left.\frac{d\sigma}{d\Omega}\right|_{\text{subs}} = r_o^2(\rho_f - \rho_s)^2 A_{xy}|E_{in}(-D)|^2|E_{out}(-D)|^2 S_{\text{subs}}(\vec{q}). \quad (10)$$

Here ρ_s is the electron density of the silicon substrate. The quantities $E_{\text{in}}(-D)$ and $E_{\text{out}}(-D)$ are the normalized electric fields at the polymer film-substrate interface (i.e., at $z=-D$ in Fig. 2) for the incident beam and the exit beam, respectively. S_{subs} is the structure factor corresponding to the interface roughness.

We now turn to an evaluation of the term $|\langle\tilde{\psi}_2|V_{\text{int}}|\psi_1\rangle|^2 = 16\pi^2 r_0^2|\langle\tilde{\psi}_2|\delta\rho_f|\psi_1\rangle|^2$, where $\delta\rho_f$ is the electron density fluctuation of the film about its average density ρ_f. The calculation is greatly simplified in the case where the scattered angle is much larger than the critical angle of the material. In this case $A_2(\beta)\approx 0$ and $A_1(\beta)\approx 1$ in the expression for $\tilde{\psi}_2$. We then have matrix element due to the interior density fluctuations given by

$$V_{\text{int},12} = 4\pi r_0 \int_S d\vec{r}_\parallel \int_{-D}^{0} dz\, \delta\rho_f(\vec{r}) e^{i\vec{q}_\parallel\cdot\vec{r}_\parallel} F(z). \quad (11)$$

Here $\vec{q}_\parallel = (\vec{k}_{2,\parallel} - \vec{k}_{1,\parallel})$, and we have defined

$$F(z) \equiv [A_1(\alpha)e^{-i(l_2^{(1)} - l_1^{(1)})z} + A_2(\alpha)e^{-i(l_1^{(1)} + l_2^{(1)})z}]. \quad (12)$$

This yields the differential scattering cross section

$$\left.\frac{d\sigma}{d\Omega}\right|_{\text{int}} = r_0^2 \int_S \int_{S'} d\vec{r}_\parallel d\vec{r}'_\parallel e^{i\vec{q}_\parallel\cdot(\vec{r}_\parallel - \vec{r}'_\parallel)} \times \int_{-D}^{0} dz \int_{-D}^{0} dz' \langle\delta\rho_f(\vec{r})\,\delta\rho_f(\vec{r}')\rangle F(z)F^*(z'). \quad (13)$$

The term involving the density correlations within the film can be re-evaluated using the relationship

$$\langle\delta\rho_m(\vec{r})\,\delta\rho_m(\vec{r}')\rangle = \frac{\langle\rho_m\rangle V}{(2\pi)^3}\int_{-\infty}^{\infty} d\vec{K} S(\vec{K}) e^{i\vec{K}\cdot(\vec{r}-\vec{r}')}. \quad (14)$$

Here $S(\vec{K})$ is the structure factor of the film, $\langle\rho_m\rangle$ is the average density of scattering units, and V is the sample volume. We take the styrene monomer as the unit scatterer. In the limit of small angles, the molecular scattering factor of a monomer units is approximately independent of q and just given by the number of electrons in a monomer. We represent this factor by (f_m). The differential scattering cross section is then given by

$$\left.\frac{d\sigma}{d\Omega}\right|_{\text{int}} = \frac{r_0^2\langle\rho_m\rangle f_m A_{xy}}{2\pi}\int_{-\infty}^{\infty} dK_z S(q_\parallel, K_z) W(K_z), \quad (15)$$

with

$$W(K_z) = \int_{-D}^{0}\int_{-D}^{0} dz dz' F(z)F^*(z')e^{-iK_z(z-z')}. \quad (16)$$

Equation (16) will only have significant amplitude when $K_z \approx q_\parallel$ to within the order of $|l_1|$ since, as seen in Eq. (12), for $l_2 D \gg 1$ the terms involving $F(z)$ will oscillate rapidly. If $S(q)$ is assumed to have no variations on this scale then it can be removed from the inside of the integral yielding

$$\left.\frac{d\sigma}{d\Omega}\right|_{\text{int}} = \frac{r_0^2\langle\rho_m\rangle f_m A_{xy}}{2\pi} S(\vec{q}_\parallel, l_2) Y(\alpha,\beta). \quad (17)$$

Thus the differential scattering cross section is proportional to the structure factor times a correction factor given by

$$Y(\alpha,\beta) = \int_{-\infty}^{\infty} dK_z W(K_z). \quad (18)$$

Note that the function Y depends on α and β through the dependence of F on the z components of the incident and reflected wave vector components, l_1 and l_2. The physical meaning of the approximation used above is that, when the length scales associated with the sample structure are sufficiently distinct from the length scales associated with the electric field variation, the standing wave does not modify the wave vector dependence of the SAXS from within the film.

We have more carefully examined the validity of the approximation made in Eq. (17) and for this purpose we solve the integration numerically in Eq. (15) for a fixed incidence angle α by taking the measured bulk $S(q)$ of polymer as the reference [10]. We also solved $Y(\alpha,\beta)$ numerically at the same angle α and calculated the structure factor that would be obtained from Eq. (17) as

$$S^*(\vec{q}_\parallel, l_2) \approx \frac{\int_{-\infty}^{\infty} dK_z S(\vec{q}_\parallel, K_z) W(K_z, l_1, l_2)}{\int_{-\infty}^{\infty} dK_z W(K_z, l_1, l_2)}. \quad (19)$$

The comparison of the reference $S(q)$ and the calculated $S^*(q)$ is shown in Fig. 3. The percentage error in calculation of $S^*(q)$ for different thickness of the polymer films is shown in the inset. The small errors even for 20-nm-thick film indicate the validity of our approximation. The important outcome of this result is that we can calculate the structure factor of the polymers in thin films from the expression in Eq. (17) by knowing the contribution in the total scattering intensity due to interior density fluctuations.

III. SMALL-ANGLE X-RAY SCATTERING

PS films (M_w=129 Kg/mol, $M_w/M_n \sim 1.05$) were deposited by spin casting on polished silicon (100) substrates. Before deposition the substrates were cleaned with piranha solution and then HF etched to remove oxide. The PS films were annealed at 170 °C for 24 h to ensure complete solvent evaporation. Measurements were performed at the 8-ID beamline at the Advanced Photon Source (APS). Samples

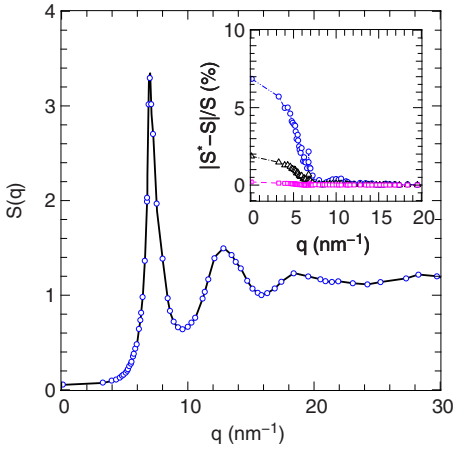

FIG. 3. (Color online) $S(q)$ for bulk PS (line) and S^* calculated for 20 nm PS film (blue circles) using Eq. (19). The inset shows the percentage error in calculation of S^* for various film thicknesses: 20 nm (blue circles dot-dot-dashed line), 38 nm (black triangles dash-dotted line), and 100 nm PS film (magenta squares dashed line).

were placed in a temperature controlled sample cell integrated with the beamline vacuum. The cell was mounted on a set of translation and rotation stages and was connected to the beamline vacuum using bellows in order to permit sample motion. An in-vacuum detector mounted on a translation stage allowed measurement of the intensity of reflected x-rays from the sample. The x-ray beam energy was 7.35 keV with a flux of approximately 10^{10} photons/s, generated by an APS undulator A 60 m upstream of the sample. A 200 μm (vertical) $\times$ 20 μm (horizontal) x-ray beam was defined by a pair of slits upstream of the sample with a second set of scatter guard slits just in front of the sample used to reduce parasitic scattering. The scattered x-rays passed through a flight path to a phosphor coupled charge coupled device (CCD) area detector (Princeton Instruments) located just outside a kapton exit window. Different length flight paths, ranging from 0.5 m to 3.5 m were used depending on the range of scattering vectors measured. A beamstop located just inside the exit window intercepted the specularly reflected x-ray beam in order to prevent parasitic scattering from the windows.

The diffusely scattered intensity depends strongly on the incident angle, α, of the x-rays. This variation with incident angle is particularly important over the range of angles between the critical angle for total external reflection of PS $\alpha_{c,PS} \approx 0.17°$ and that of Si $\alpha_{c,Si} \approx 0.24°$ at an energy 7.35 keV. In this range there is interference inside the PS film between the incident beam and the beam reflected by the Si. Some particular values of α yield a standing-wave condition resulting in an electric field intensity distribution with the intensity peaked within the interior of the film and nearly zero at the surface. This is the case for the 20-nm- and 38-nm-thick PS films and the field distributions are shown in [Figs. 4(a) and 4(b)]. For thicker films it is possible to obtain higher-order standing waves yielding multiple peaks. This is the case for the thicker films as shown in Figs. 4(c) and 4(d) for 70-nm- and 114-nm-thick PS films. At these conditions nearly all the intensity comes from the interior of the film;

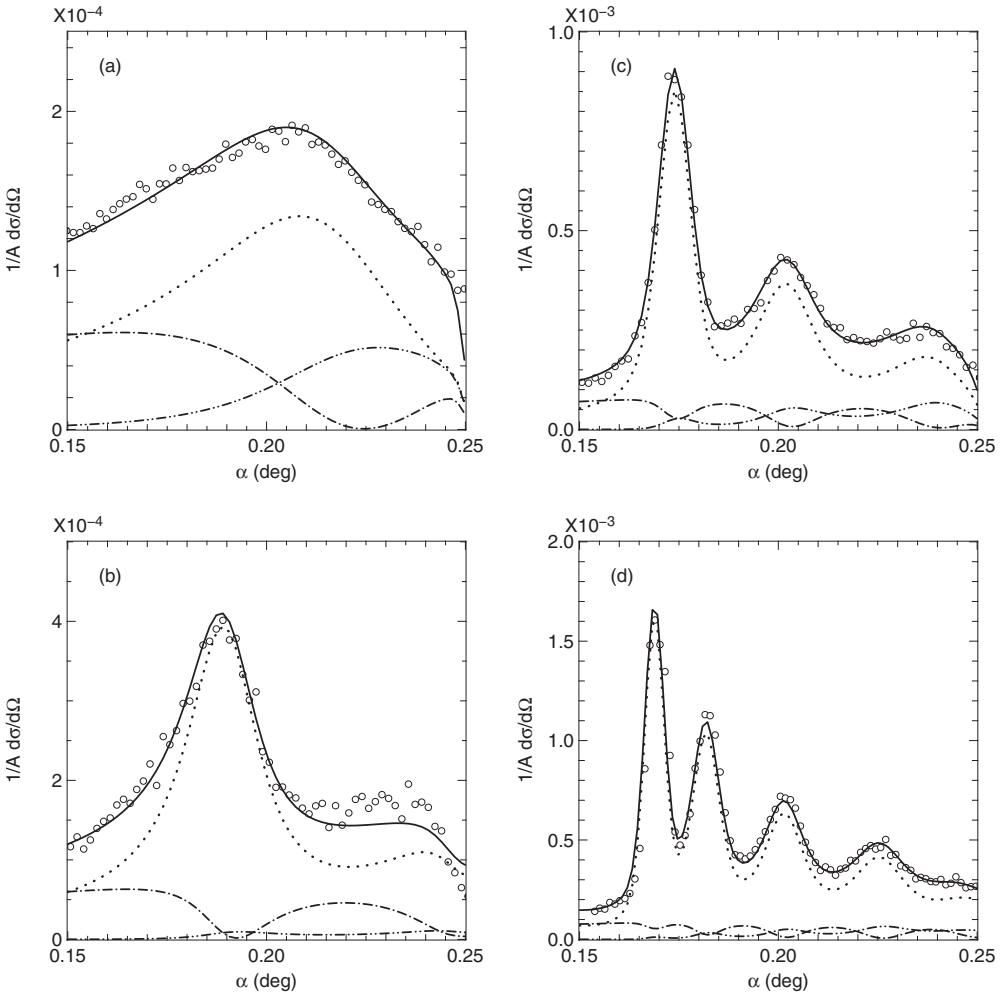

FIG. 4. Diffuse scattering cross section at $\vec{q}_{\|}=1.525\ \mathrm{nm}^{-1}$ and $q_z=0.616\ \mathrm{nm}^{-1}$ as a function of incident angle for (a) 20-nm-, (b) 38-nm-, (c) 70-nm-, and (d) 114-nm-thick PS films on Si at 160 °C. Symbols are experimental data and the solid line is the fit. The surface (dash-dotted line), substrate (dot-dot-dashed line), and interior (dotted line) scattering contributions are shown separately.

the surface and the substrate scattering is suppressed.

At any given value of the scattered angle we can model the measured diffuse scattering as a function of incident angle using the method described above. This model will require three adjustable parameters describing the magnitude of the scattering intensity from the surface, interior, and substrate. In order to interpret our experimental data, these parameters were varied to yield the best fit to the data as determined by least-squares minimization. The intensity due to surface scattering can also be calculated following Eq. (9), and this calculated result agreed with the best-fit value to the variation with incident angle. The two other adjustable parameters are the intensity of the interior diffuse scattering from the film [calculated using Eq. (17)] and the substrate scattering [calculated using Eq. (10)]. The latter is negligible compared to the former at large $\vec{q}$ but becomes important in the small $\vec{q}$ region. Since we do not have a good model for the origin of the substrate scattering, we exclude data where the substrate scattering exceeds the contribution of the interior of the film at an α corresponding to the strongest peak of the standing wave inside the film.

In Fig. 5 the interior contribution to $S(q)$ is presented for a number of different film thicknesses. The data are averaged over the orientation of $\vec{q}$. Note that it was not possible to obtain data for q values lower than around 1 nm^{-1} since at small q the surface scattering is too strong relative to the bulk and cannot be accurately subtracted. The orientation dependence of $S(\vec{q})$ at $q=2\ \mathrm{nm}^{-1}$ for various film thicknesses is also shown in the inset to Fig. 5. The scattering was found to vary by around 20% with orientation in the thinnest film but had little variation in thicker films. In bulk PS the thermal diffuse scattering at low q is due to density fluctuations and is proportional to the magnitude of the isothermal compressibility [11,12]. Thus as $q\rightarrow 0$ one should find

$$S(0)=\langle\rho_m\rangle f_m k_B T\kappa_T. \tag{20}$$

Here k_B is the Boltzmann constant, T is the temperature, and κ_T is the isothermal compressibility. Note that this relationship is only valid in thermal equilibrium and thus only applies for temperatures above the glass transition, T_g. For thick films Eq. (20) holds at small q and yields the expected value of κ_T. In bulk PS there is an increase in $S(q)$ at larger q. This rise was interpreted by Roe and Curro [11,12] as resulting from quasistatic correlations between the monomers. Roe and Curro fit their data to the expression

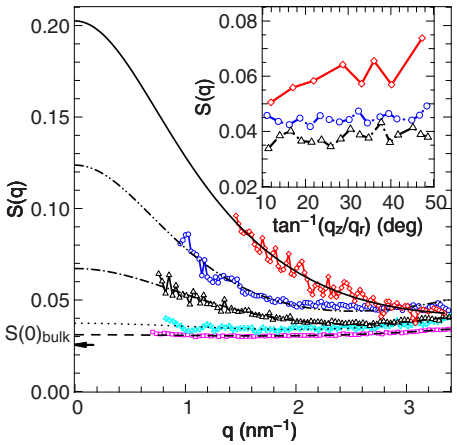

FIG. 5. (Color online) $S(q)$ for film thicknesses of 10 nm (red diamonds and black solid line), 20 nm (blue circles and black dot-dot-dashed line), 38 nm (black triangles and dash-dotted line), 57 nm (cyan crosses and black dotted line), and 105 nm (magenta squares and black dashed line) at 160 °C. Lines represent fits, symbols represent the measured data. The arrow marks the bulk $S(0)$. Inset: variation in $S(q)$ with orientation at $q=2$ nm^{-1} for film thicknesses of 10 nm (red diamonds solid line), 20 nm (blue circles dot-dot-dashed line), and 38 nm (black triangles dash-dotted line).

$$S(q) = S(0)\exp(bq^2). \tag{21}$$

This form fits our $S(q)$ data for thick films quite well but fails for films thinner than 60 nm where there is an additional rise in intensity at small q. This behavior is qualitatively similar to the structure factor calculated in Monte Carlo simulations of thin polymer films by Binder [13] and also to the predictions of the Gaussian string model of Schweizer and Curro [14,15].

To account for this scattering we employ a functional form inspired by the Gaussian string model:

$$S(q) = \frac{S(0)}{1+\xi^2 q^2} + Aq^2. \tag{22}$$

Here ξ represents a density fluctuation screening length. The Gaussian string model [14,15] would only predict the first term in Eq. (22). The quadratic term represents the quasistatic component. This model then has three adjustable parameters, κ_T, ξ, and A. The lines in Fig. 5 represent fits using this model. Here, we are showing the data taken at $T=160$ °C, well above T_g. We also have taken data as a function of temperature for 105 and 38 nm PS films and data for both the films are found to be similar at temperatures above bulk $T_g \approx 100$ °C of PS.

The thickness dependence of κ_T and ξ are shown in Fig. 6(a) for 160 °C. The compressibility shows no change for $D/R_g > 6$ and then shows a sharp increase with decreasing D up to about seven times for the thinnest film. Note, however, that the compressibility values for the thinner films have large uncertainties since they involve an extrapolation of the data back to $q=0$. The thickness dependence of the compressibility can be reasonably well described by the functional form:

$$\kappa_T(D) = \kappa_T^{\text{bulk}}[1 + C_1 \exp(-D/D_0)]. \tag{23}$$

The extrapolated value of κ_T for an infinitely thick film is consistent with the bulk value. The temperature dependence of κ_T is also consistent with that of the bulk. The values required to fit the data of compressibility as a function of thickness are $D_0 = 18.9 \pm 6.6$ nm and $C_1 = 13.6 \pm 3.8$. The variable ξ^2 is also plotted together with the compressibility in Fig. 6(a) to show the similar thickness dependence as compressibility.

Since in the low q limit $S(q)$ is proportional to the compressibility, the temperature dependence of $S(0)$ gives the temperature dependence of κ_T. One well-established signature of the glass transition in polymers is a discontinuity in

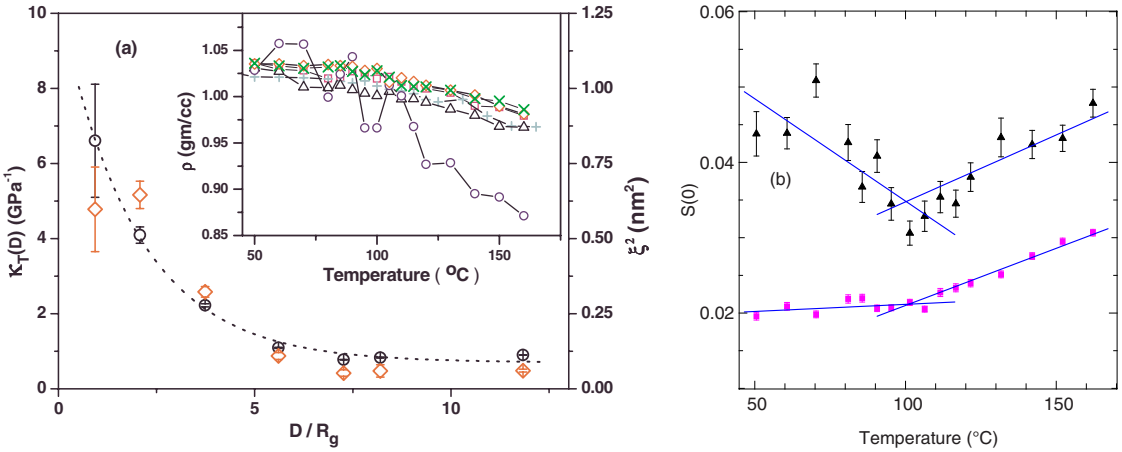

FIG. 6. (Color online) (a) Thickness dependence of fitting parameters. The left side scale is for the film compressibility $\kappa_T(T)$ and the right side scale is for the square of the correlation length ξ^2. The black circles show the measured film compressibility. Thicknesses are normalized by the bulk radius of gyration, R_g. Red diamonds show the square of the correlation length obtained from the fitting. The line shows fit using Eq. (22). Inset: density vs temperature for thicknesses of 20 nm (blue circles), 38 nm (black triangles), 57 nm (cyan crosses), 70 nm (red diamonds), 78 nm (green rotated crosses), and 105 nm (magenta squares). (b) $S_\rho(0)$ plotted as a function of temperature for 38 nm (black triangles) and 105 nm (magenta squares) PS films.

the slope of κ_T with temperature. Hence, by measuring the temperature dependence of $S(0)$ and looking for a discontinuity in slope one can measure the glass transition temperature (T_g). This method of determining T_g was applied by Roe and Curro to bulk PS [11].

The variation in T_g with film thickness for thin PS films has been a question of considerable interest [16] and thus grazing incidence small angle scattering (GISAXS) measurements have the potential to shed light on this issue. We have extracted T_g for our films by fitting the temperature dependence of $S(0)$ [which is proportional $\kappa_T(T)$] to two lines; one for the low temperature portion of the curve and one for the high-temperature portion. The value of T_g is then taken from the intersection of the lines. This is shown in Fig. 6(b). For the 38 and 105 nm PS films we find $T_g = 100 \pm 3$ °C and $T_g = 101 \pm 9$ °C, respectively. However, based on previous work by Keddie *et al.* [17], one would only expect a depression of T_g of 4 °C and the errors on present data are too large to resolve any meaningful thickness-dependent changes.

IV. WIDE ANGLE X-RAY SCATTERING RESULTS

At small angles, the interior scattering is dominated by collective density fluctuations within the polymer. At large angles this scattering comes from correlations between the positions of the individual polymer chains. Thus, measurements in the WAXS regime probe the local molecular interactions. In order to perform WAXS measurements the experimental geometry was modified slightly. The vacuum flight path before the detector was removed and a large area detector was placed directly against the exit window of the vacuum space.

Wide angle scattering results for three different film thicknesses at fixed incident angle are shown in Fig. 7. For thick films, the WAXS is isotropic and similar to previous bulk measurements by Londono *et al.* [18]. The WAXS from PS is expected to show a number of liquidlike correlation peaks. Only the first of these is visible due to the limited access range of the windows. This first peak, sometimes referred to as the prepeak or polymerization peak, occurs in a number of polymer melts and has been shown to be due to correlations between the side chains, which in the case of PS would be the pendant phenol rings [19]. As seen in the figure, for thick PS films (114 nm) the ring of scattering corresponding to the prepeak does not depend on the azimuthal angle. For thinner films the ring of scattering becomes nonuniform and begins to collapse into a peak at an azimuth of 90° and the peak becomes more intense. For the thinnest film examined (20 nm) scattering around the ring has nearly vanished and moved to a single broad peak at 90°.

The existence of this peak implies that for thin films the orientation of the polymers is no longer random, but the polymers are aligned relative to the surface. It is not too surprising that for sufficiently thin films the polymer chains choose to lie preferentially parallel to the surface. However, the existence of such an orientation would invalidate some of the simplifying approximations used to model polymer films, such as that of Silberberg [20] which assume that the only

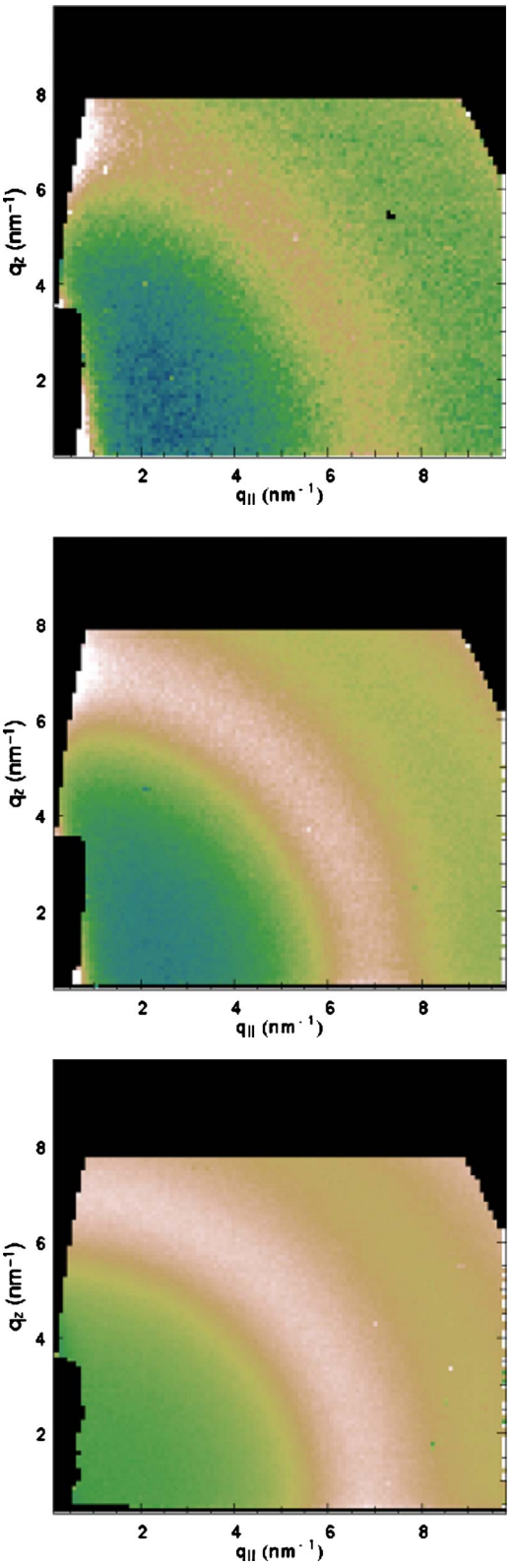

FIG. 7. (Color online) Wide angle scattering from PS films at 160 °C for 20 nm (top), 38 nm (center), and 114 nm (bottom) thick films.

effect of a surface on polymer orientation is to reflect the random polymer configuration about the surface plane. It is also interesting that, as a function of film thickness, the tran-

sition between the oriented state and the random liquid state is continuous. Previous studies of the prepeak using both molecular dynamics [21] and vacuum ultraviolet (vuv) spectroscopy [22] have shown that this peak arises from an end-to end parallel alignment of the pendant phenol rings in PS. The orientation of the scattering peak along the q_z direction implies that the phenol rings are oriented along the z direction implying a stacking of phenol rings in this direction, most likely from different polymer chains.

V. DISCUSSION AND CONCLUSIONS

It is clear from both the small-angle and wide-angle scattering measurements described above that there is a change in the internal structure of the PS films as they are made thinner. We sketch here one scenario for what may be happening. In thick films, the effect of the surface is largely as described by Silberberg [20], the chain conformations are reflected at the polymer-vacuum and polymer-substrate surfaces as if by a mirror.

In thinner films, effects associated with the interface become more important. One such effect is the failure of the random phase approximation. The basis of this approximation is that within a dense polymer melt the chain conformation adopts a random walk rather than a self-avoiding random walk due to the fact that most of the monomer units surrounding a given section of a polymer chain belong to different chains. However, when the presence of the interfaces causes sufficient folding back of a given polymer chain onto itself this increases the likelihood that adjacent monomers come from the same chain. Thus, one would expect that for thin enough films the configuration of the polymer chains should start to resemble a self-avoiding random walk rather than a simple random walk. This would imply that the polymer chain size would begin to swell, leading to a decrease in density. Such a density decrease has been seen in thin films by x-ray reflectivity studies [23].

For films thin enough that there is only partial interpenetration of the chains, one would expect that the density of the polymer will vary with lateral position on the surface. Near the center of a polymer-coil, interpenetration with other chains is a minimum due to backfolding. In this region the configuration resembles a self-avoiding random walk leading to a lower density. Near the extremities of a coil interpenetration is higher leading to a random-walk configuration and higher density. This lateral density variation is consistent with the observation from the GISAXS of a peak in $S(q)$ at small q. This model would also predict that the intensity of this peak increases as the film thins, which is also consistent with the scattering measurements. As shown above and also discussed elsewhere [23] this peak is predicted both from Monte Carlo simulations and analytic Gaussian thread calculations.

The WAXS results show that for very thin films the scattering is no longer isotropic. A plausible explanation for this orientation of the polymer chains relative to the surface is that the reflection of a polymer chain from an interface increases the configurational energy of the chain. Real polymer chains are not freely jointed. They only approximate this ideal state over length scales longer than the persistence length. Thus, whenever the chain reflects from a surface there is an increase in the energy of the chain for a chain segment of order the persistence length. Even when the radius of gyration of the chain is large compared to the persistence length, the additional energy may be enough to alter the equilibrium configuration of the chain so that it preferentially lies parallel to the surface so as to minimize reflections. This would then lead to the observed change from an isotropic angular dependence of the GIWAXS for thick films to a peaking of the scattering for decreasing film thickness.

In conclusion, we have shown that the structure factor corresponding to the density fluctuations within the interior of the thin films can be extracted by measuring wide-angle and small-angle diffuse scatterings. The use of standing-wave technique is particularly useful to enhance the contribution of the interior scattering in comparison to surface or interface scattering. As the films become even thinner, both SAXS and WAXS show that the polymer coils become oriented parallel to the surface. However, for sufficiently thin films the idea of an interior structure as distinct from a surface structure becomes untenable. Under this circumstance, the formalism developed above for isolating surface and bulk structure factors is no longer workable. Furthermore, the structure at the substrate interface will also become an increasingly strong contribution to the scattering and it will become impossible to separate this scattering from the scattering due to the polymer. Under such circumstances it becomes critical to obtain an extremely flat and clean substrate so as to eliminate, to the extent possible, this contribution to the scattering. Fortunately with modern semiconductor preparation techniques this is possible with materials such as single crystal silicon. However, even in the best case of a perfectly flat substrate, the scattering from the polymer will include contributions from the interior and the interface which cannot be separated from an analysis of the scattering alone. The best approach would then be a comparison of the measured scattering with predictions from theoretical simulations. In this case the formalism developed above would be crucial for making this comparison.

ACKNOWLEDGMENTS

We would like to acknowledge K. Binder and K. Schweizer for useful discussions, A. R. Sandy and S. Narayanan for experimental support at the beamline and useful discussions, H. Gibson for his expert technical work, and A. Habenschuss for sharing data on bulk PS melts. This work is supported by NSF Grant No. DMR-0209542. Use of the Advanced Photon Source at Argonne National Laboratory was supported by (U.S.) Department of Energy, Office of Science, Office of Basic Energy Sciences, under DOE Contract No. DE-AC02-06CH11357.

[1] J. Wang, M. J. Bedzyk, and M. Caffrey, Science **258**, 775 (1992).
[2] S. K. Sinha, E. B. Sirota, S. Garoff, and H. B. Stanley, Phys. Rev. B **38**, 2297 (1988).
[3] M. Rauscher, T. Salditt, and H. Spohn, Phys. Rev. B **52**, 16855 (1995).
[4] V. Holý, J. Kubena, I. Ohlidal, K. Lischka, and W. Plotz, Phys. Rev. B **47**, 15896 (1993).
[5] M. Tolan, *X-ray Scattering from Soft-Matter Thin Films* (Springer, Berlin, 1999).
[6] J. Daillant and A. Gibaud, *X-ray and Neutron Reflectivity and Scattering* (Springer, Berlin, 1999).
[7] L. G. Parratt, Phys. Rev. **95**, 359 (1954).
[8] L. Lurio, H. Kim, A. Ruhm, J. Basu, J. Lal, S. Sinha, and S. G. J. Mochrie, Macromolecules **36**, 5704 (2003).
[9] J. Wang, M. Tolan, O. H. Seeck, S. K. Sinha, O. Bahr, M. H. Rafailovich, and J. Sokolov, Phys. Rev. Lett. **83**, 564 (1999).
[10] A. Habenschuss (private communication).
[11] R. Roe and J. Curro, Macromolecules **16**, 428 (1983).
[12] R. Roe, *Methods of X-ray and Neutron Scattering in Polymer Science* (Oxford, New York, 2000).
[13] K. Binder, Physica A **200**, 722 (1993); *Fourth International Bar-llan Conference on Frontiers in Condensed-Matter Physics* (Bar-Ilan, Israel, 1993).
[14] K. S. Schweizer and J. G. Curro, Chem. Phys. **149**, 105 (1990).
[15] K. S. Schweizer, in *Advances in Chemical Physics*, edited by I. Prigogine and S. A. Rice (Wiley and Sons, New York, 1997), Vol. 98, pp. 1–142.
[16] J. A. Forrest, Eur. Phys. J. E **8**, 261 (2002).
[17] J. Keddie, R. Jones, and R. A. Cory, Europhys. Lett. **27**, 59 (1994).
[18] J. D. Londono, A. Habenschuss, J. G. Curro, and J. J. Rajasekaran, J. Polym. Sci., Part B: Polym. Phys. **34**, 3055 (1996).
[19] M. H. Kim, J. D. Londono, and A. Habenschuss, J. Polym. Sci., Part B: Polym. Phys. **38**, 2480 (2000).
[20] A. Silberberg, J. Colloid Interface Sci. **90**, 86 (1982).
[21] B. Vorselaars, A. V. Lyulin, and M. A. J. Michels, Macromolecules **40**, 6001 (2007).
[22] S. Chattopadhyay, A. Datta, A. Giglia, N. Mahne, A. Das, and S. Nannarone, Macromolecules **40**, 9190 (2007).
[23] M. K. Mukhopadhyay, X. Jiao, L. B. Lurio, Z. Jiang, J. Stark, M. Sprung, S. Narayanan, A. R. Sandy, and S. K. Sinha, Phys. Rev. Lett. **101**, 115501 (2008).